Chirp of the single attosecond pulse generated by a polarization gating

Zenghu Chang*
Department of Physics, Kansas State University, Manhattan, Kansas 66506, USA
(Received 18 September 2004; published 28 February 2005)

The chirp of the xuv supercontinuum generated by a polarization gating is investigated by comparing three-dimensional nonadiabatic numerical simulations with classical calculations. The origin of the chirp is the dependence of the energy gain by an electron on the return time. The chirp is positive and its value is almost the same as that when a linearly polarized laser is used. Although the 250-eV-wide supercontinuum corresponds to a single attosecond pulse, the shortest duration of the pulse is limited by the chirp. By compensating the positive chirp with the negative group velocity dispersion of a Sn filter, it is predicted that a single 58-as pulse can be generated.

DOI: 10.1103/PhysRevA.71.023813 PACS number(s): 42.65.Ky, 42.65.Re

The shortest optical pulse generated so far is 250 as, which was from high-order harmonic generation using 5-fs linearly polarized laser pulses [1]. The pulse is still significantly longer than 1 atomic unit of time, i.e., 24 as, which is the time scale of electron motion in atoms. For studying and controlling such motion with high precision, it is desirable to have even shorter single attosecond pulses. A typical high-order harmonic spectrum shows that the intensities fall off drastically for the first few orders, then remain almost constant for many orders, forming a plateau, and finally cut off abruptly for the highest orders [2,3]. When the carrier-envelope phase of the 5-fs laser pulse is close to zero (a cosine pulse), the spectrum in the cutoff region is a continuum, which was extracted by spectral filtering to produce the single attosecond pulse [1,4–7]. The pulse duration was limited by the bandwidth of the continuum, which is less than 20 eV [7], and by the bandwidth of the multilayer mirror, which is 5.1 eV full width at half maximum [5].

The generation of a single attosecond pulse less than 100 as in duration requires a continuum broader than ~40 eV [8]. The exact value of the bandwidth depends on the pulse shape and the phase of the pulse. Recently, it has been demonstrated experimentally that a supercontinuum covering the plateau and the cutoff region is generated using a laser pulse with a time-dependent ellipticity. The laser pulse is composed of two circularly polarized 8-fs pulses [9]. Theoretically, a supercontinuum wider than 100 eV can be generated by a polarization gating using 5-fs laser pulses [10]. So far, a significant amount of effort has been devoted to theoretical and experimental studies of polarization gating [11–15]. However, the chirp of pulses generated with this technique is still not well understood. In this communication, the spectral phase of the supercontinuum generated by a polarization gating is investigated, and the chirp of the attosecond pulse as a result of phase variation is analyzed.

The high-order harmonic spectra and phases are studied by numerical simulations utilizing a three-dimensional nonadiabatic technique [16] adapted for harmonic generation using a driving pulse with a time-dependent ellipticity [10]. Helium was chosen as the target gas. First, the harmonic generation from a single atom was simulated. Then the macroscopic harmonic signal was calculated by solving a three-dimensional wave equation for the harmonic field. It was assumed that the laser pulse with a time-dependent ellipticity is formed by the superposition of a left- and a right-circularly polarized Gaussian pulse [14,15]. The peak field amplitude E_0, carrier frequency ($\omega=2\pi/2.5$ rad/fs), pulse duration ($\tau_p=5$ fs), and carrier-envelope phase ($\phi=\pi/2$) are the same for the two pulses. The delay between them is T_d, which is two times the optical period, i.e., $T_d=5$ fs. The electric field of the combined pulse is $\mathbf{E}(t)=E_x(t)\hat{\mathbf{x}}+E_y(t)\hat{\mathbf{y}}$. $\hat{\mathbf{x}}$ and $\hat{\mathbf{y}}$ are unit vectors in the x and y directions, respectively. The two components of the laser field are

$$E_x(t)=E_0\hat{\mathbf{x}}\left\{\exp\left[-2\ln(2)\left(\frac{t-T_d/2}{\tau_p}\right)^2\right]+\exp\left[-2\ln(2)\left(\frac{t+T_d/2}{\tau_p}\right)^2\right]\right\}\cos(\omega t+\phi),$$

$$E_y(t)=E_0\hat{\mathbf{y}}\left\{\exp\left[-2\ln(2)\left(\frac{t-T_d/2}{\tau_p}\right)^2\right]-\exp\left[-2\ln(2)\left(\frac{t+T_d/2}{\tau_p}\right)^2\right]\right\}\sin(\omega t+\phi). \quad (1)$$

The laser field is linearly polarized at $t=0$, while the ellipticity increases with $|t|$.

The single-atom response was calculated by the nonadiabatic Lewenstein model [16,17]. When the ellipticity of the driving pulse changed with time, the two transverse components of the dipole moment were calculated separately. Calculations showed that the amplitude of the harmonic spectrum along $\hat{\mathbf{y}}$ was much smaller than that along $\hat{\mathbf{x}}$. Thus, only the latter was considered. The dipole moment along the $\hat{\mathbf{x}}$ direction of the laser field was calculated by the integral

*Electronic address: chang@phys.ksu.edu

$$x(t) \approx i\int_0^\infty d\tau\left(\frac{\pi}{\varepsilon + i\tau/2}\right)^{3/2} d_x^*[\mathbf{p}_s(t,\tau) - \mathbf{A}(t)]e^{-iS(\mathbf{p}_s,t,\tau)} \times \{\mathbf{E}_x(t-\tau)\cdot d_x[\mathbf{p}_s(t,\tau) - \mathbf{A}(t-\tau)] + \mathbf{E}_y(t-\tau)\cdot d_y[\mathbf{p}_s(t,\tau) - \mathbf{A}(t-\tau)]\}|a(t)|^2 + \text{c.c.}, \quad (2)$$

where $\mathbf{A}(t)$ is the vector potential of the laser field, ε is a small number, $I_p = 24.59$ eV is the ionization potential of the helium atom, and $a(t)$ is the ground-state amplitude as calculated by the Ammosov-Delone-Krainov (ADK) theory [18,19]. The helium atom was chosen to avoid significant depletion of the ground state at the calculated intensity 1.4×10^{15} W/cm^2. The field-free dipole transition matrix elements between the ground state and the continuum state are

$$d_x^*[\mathbf{p}_s(t,\tau) - \mathbf{A}(t)] = -i\frac{2^{7/2}}{\pi}\alpha^{5/4}\frac{p_{s,x}(t,\tau) - A_x(t)}{\{[p_{s,x}(t,\tau) - A_x(t)]^2 + [p_{s,y}(t,\tau) - A_y(t)]^2 + \alpha\}^3}, \quad (3)$$

$$d_y^*[\mathbf{p}_s(t,\tau) - \mathbf{A}(t)] = -i\frac{2^{7/2}}{\pi}\alpha^{5/4}\frac{p_{s,y}(t,\tau) - A_y(t)}{\{[p_{s,x}(t,\tau) - A_x(t)]^2 + [p_{s,y}(t,\tau) - A_y(t)]^2 + \alpha\}^3}. \quad (4)$$

The two components of the canonical momentum of the electron corresponding to a stationary phase are calculated by $p_{s,x}(t,\tau) = \int_{t-\tau}^t dt'' A_x(t'')/\tau$, and $p_{s,y}(t,\tau) = \int_{t-\tau}^t dt'' A_y(t'')/\tau$. Finally, the quasiclassical action of the electron is calculated by

$$S(\mathbf{p}_s,t,\tau) = I_p\tau - \frac{1}{2}[p_{s,x}{}^2(t,\tau) + p_{s,y}{}^2(t,\tau)] + \frac{1}{2}\int_{t-\tau}^t dt''[A_x{}^2(t'') + A_y{}^2(t'')] \quad (5)$$

where $\alpha = 2I_p$.

The macroscopic harmonic signal from all the atoms in the target was calculated by solving the wave propagation equation in the moving frame of the harmonic field $E(\omega_H, r, z')$ in the frequency domain [16],

$$\nabla_\perp^2 E(\omega_H,r,z) - \frac{2i\omega_H}{c}\frac{\partial E(\omega_H,r,z)}{\partial z} = -\omega_H^2\mu_0 P_{\text{nl}}(\omega_H,r,z) \quad (6)$$

where ω_H is the frequency of the harmonic field, r is the transverse coordinate, z is the propagation coordinate in the moving frame which has the same value as in the laboratory frame, c is the speed of light in vacuum, and μ_0 is the permeability of free space. The nonlinear polarization $P_{\text{nl}}(\omega_H,r,z) \propto x(\omega_H,r,z)$. $x(\omega_H,r,z)$ is the dipole moment of an atom at (r,z) that is the Fourier transform of the $x(t,r,z)$ calculated with Eq. (2) for the atom.

The laser is a Gaussian beam propagating in the z direction. Cylindrical symmetry with respect to the z axis is assumed. The beam waist at the focus is $w_0 = 25$ μm, which gives a Rayleigh range $z_R = 2.6$ mm. A 1-mm-long gas target is centered at 2 mm after the laser focus. The atomic density of the target is assumed to be a constant. Equation (6) is solved numerically for each frequency in a spatial grid. The single-atom dipole moments at the grid points are calculated first and then are entered into Eq. (6) through the polarization $P_{\text{nl}}(\omega_H,r,z)$. The output spectrum is calculated by adding up the power spectrum at each transverse point at the exit of the

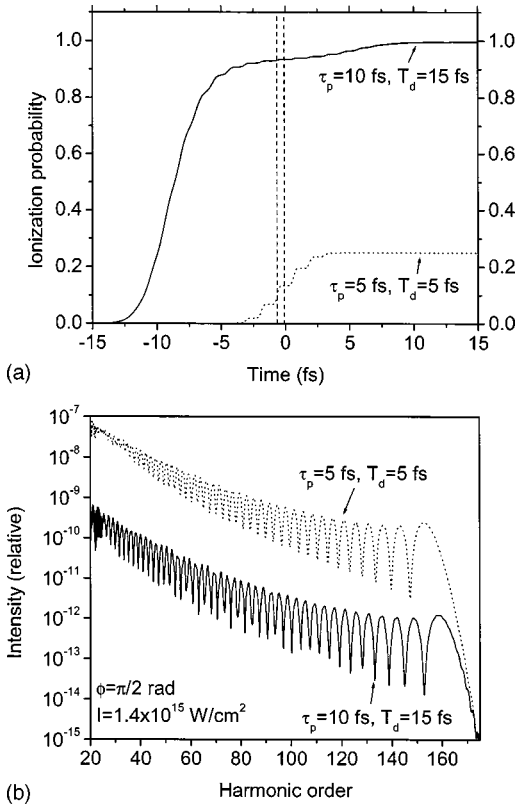

FIG. 1. (a) The ionization probabilities of a helium atom in laser fields with a time-dependent ellipticity. The laser pulse is formed by the combination of a left- and a right-hand circularly polarized pulse. Solid line: both circular pulses are 10 fs and the delay between them is 15 fs. The dotted line is obtained when the pulse duration is 5 fs and the delay is 5 fs. The intensity at $t=0$ is 1.4×10^{15} W/cm^2. The carrier-envelope phase of the laser pulse is $\pi/2$ rad. The high harmonics are generated within the time interval between the two dashed lines. (b) The single-atom high-order harmonic spectra. The dotted and the solid lines are the results obtained with 5- and 10-fs laser pulses, respectively.

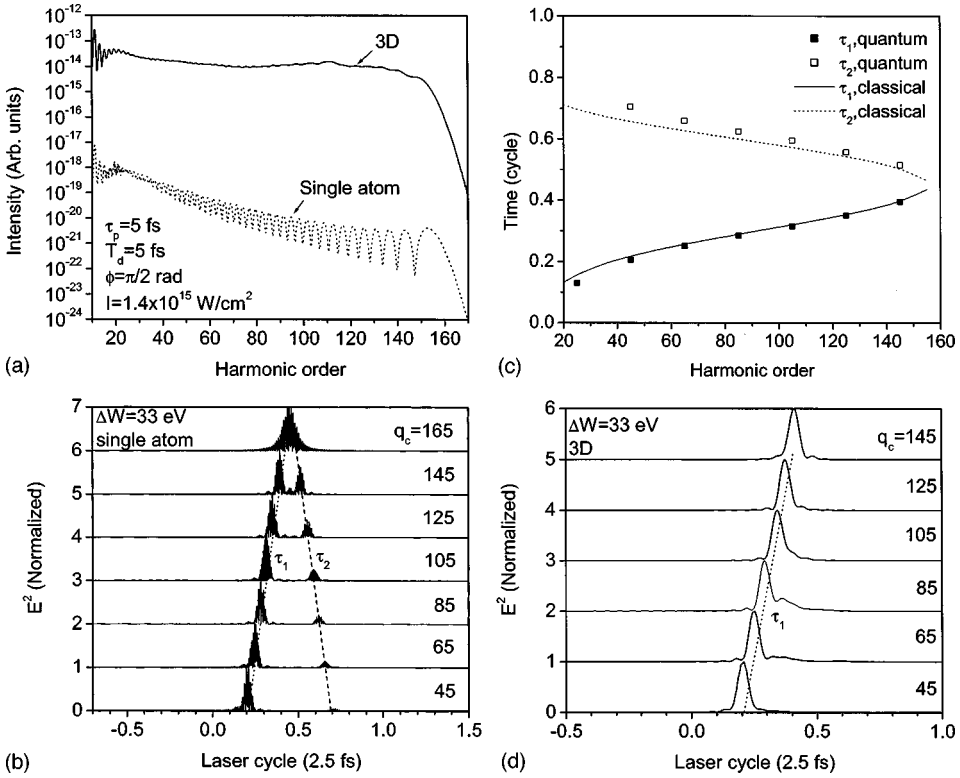

FIG. 2. (a) The high-order harmonic spectra. The dotted and the solid lines are the results of the single-atom calculation and three-dimensional simulations, respectively. (b) The high-harmonic pulses centered at different frequencies emitted from a single atom. τ_1 and τ_2 represent the short and long trajectories, respectively. The spectrum window is 33 eV. (c) The recombination time of the electrons with short and long trajectories. Recombination in other laser cycles is suppressed by the large ellipticity of the field. (d) The pulses from the three-dimensional propagation simulations.

target. To obtain the harmonic pulse in the time domain, a square spectral window is applied to the harmonic spectrum at each transverse point at the exit of the target, and inverse Fourier transforms are performed to obtain the harmonic pulse for that point. The pulses of all the points are summed up to yield the final pulse intensity.

The duration of the circularly polarized laser pulses, 5 fs, for forming the pulses with a time-dependent ellipticity is chosen to avoid significant ionization of the helium atom by the leading edge of the pulse. Figure 1(a) shows the ionization probabilities of the atom with 5- and 10-fs pulses calculated by the ADK theory [18,19]. The laser intensities are the same for both pulses at time $t=0$ fs where the laser is linearly polarized. The high harmonics are generated by electrons freed at the time interval between the two dashed lines. The ionization probability at $t=0$ is 13.4% for the 5-fs pulses that is much less than that with the 10-fs pulses (93.4%). As a result, the intensity of harmonics generated by the 5-fs pulses is more than two orders of magnitude higher than that produced by the 10-fs pulses, as shown by Fig. 1(b). The delay between the two 10-fs pulses is 15 fs, which was chosen to yield a similar spectrum as that from the 5-fs lasers. Decreasing the delay reduces the ionization but produces more than one attosecond pulse when the propagation effects are taken into account.

The lower ionization probability with the 5-fs lasers leads to a longer coherent length for high-harmonic generation. When the target gas pressure is 1.8 Torr, the coherent length for the cutoff order, i.e., 160th, is 1.03 mm with the 5-fs laser, which is almost the same as the target length (1 mm). For the same harmonics, the coherent length is 0.148 mm with the 10-fs laser pulses. The differences in the coherent lengths introduce another factor of 45 difference in harmonic intensity in favor of the 5-fs lasers, because the harmonic intensity scales with the square of the coherent length. Thus, it is clear that the shortest laser pulses should be used for generating single attosecond pulses with a polarization gating.

The simulations of the three-dimensional (3D) propagation of the laser and harmonic fields were done for only the 5-fs laser pulse. The transverse plasma density variation may cause self-focusing to the laser beam, while the time-dependent plasma density may introduce self-phase-modulation to the laser pulse. These effects will be investigated in detail in the future. The simulations in this work ignore these plasma effects, which are valid for low target gas pressures. The harmonic spectrum from the 3D propagation is different from the single-atom one, as shown in Fig. 2(a). We focus on the single-atom spectrum first. The intensity of the single-atom spectrum generated by the 5-fs laser is modulated throughout the plateau and the cutoff region. With the increase of frequency, the separation of peaks decreases but the modulation depth increases. To understand this spectral feature, a square window with a width of 33 eV was applied to the harmonic spectrum in Fig. 2(a) to select sections of spectrum entered at several different harmonic orders. These spectra were Fourier transformed to yield harmonic pulses in the time domain. This technique allows us to study the emission time of harmonics within the selected spectral window. The results are shown in Fig. 2(b). For clarity of presentation, the pulse intensities are normalized. It is clear that for plateau harmonics, two attosecond pulses are emitted in the laser cycle after $t=0$. For the cutoff order, the two pulses overlap in time. Although the laser pulses have many cycles, the fast change of ellipticity allows harmonic generation only in *one* laser cycle. The harmonic emissions

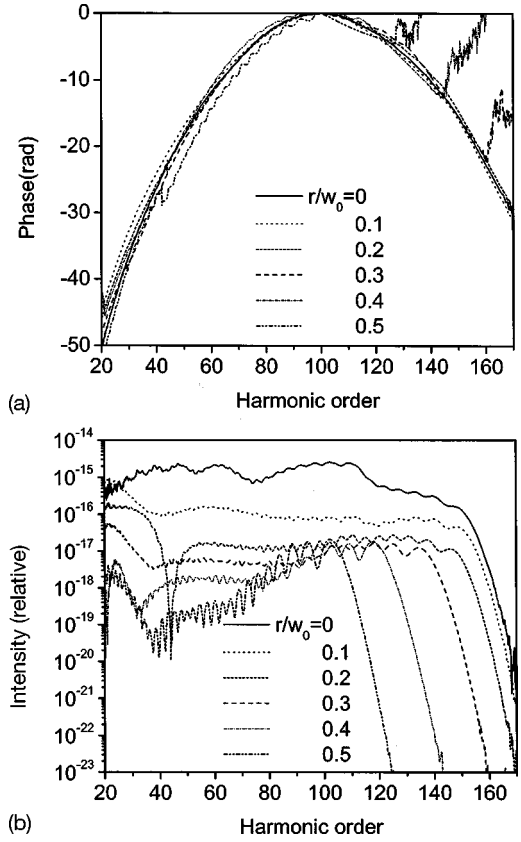

FIG. 3. (a) The phases and (b) the intensities of the high-harmonic field at different radial positions of the exit plane.

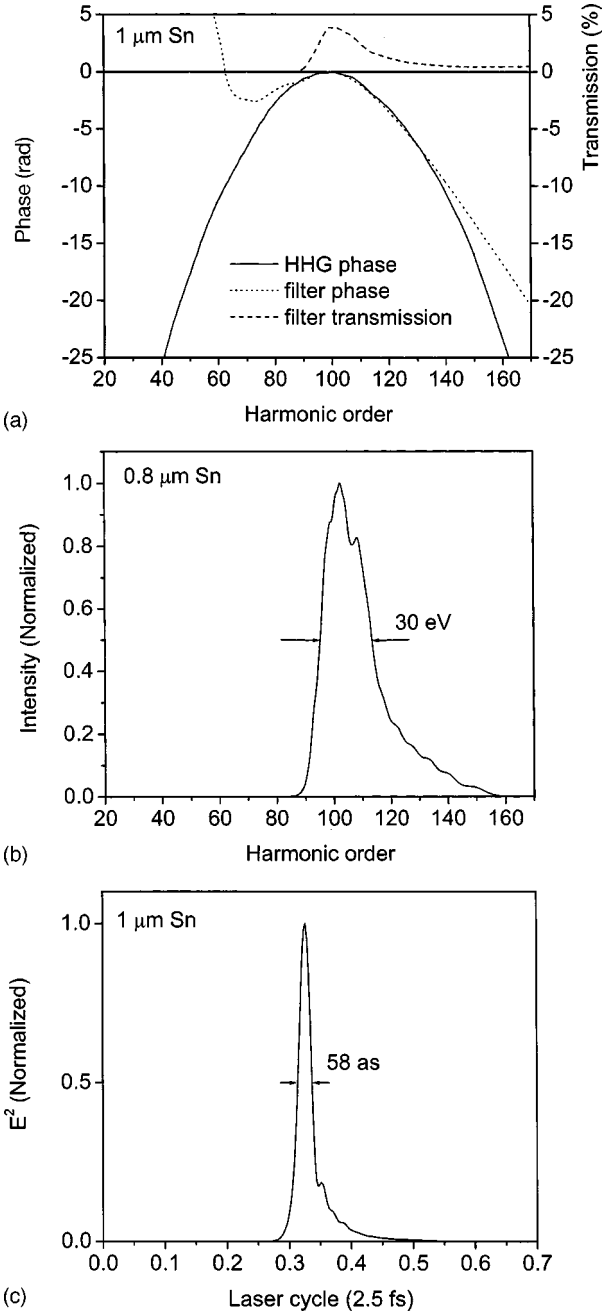

FIG. 4. (a) Comparison of the phases between the Sn filter and the high-harmonic field at the center of the exit plane. (b) The intensity of the high-harmonic spectrum and (c) the shape of the attosecond pulse after the Sn filter.

in other laser cycles are suppressed by the large ellipticity of the laser field. In fact, the single-atom spectrum resembles that in [20], where single-cycle, 2.4-fs, linearly polarized laser pulses centered at 800 nm were used. For lower-order harmonics, the ellipticity at the time when the second pulses are generated is significantly larger than that of the first pulses. This leads to the diminishing of the second pulses.

Since the ellipticity is small for the laser cycle around $t=0$, it is expected that the harmonic generation process in that cycle is similar to that occurring in a linearly polarized laser field which has been studied extensively [21,22]. Just as in a linear laser field, for a given central frequency the first pulse corresponds to the short trajectory (labeled by τ_1) and the second one corresponds to the long trajectory (labeled by τ_2). The modulation in the single-atom spectrum is the result of interference between the two pulses. The intensity of the second pulse diminishes with decrease of the central frequency. This leads to a reduction of the modulation depth at low harmonic orders. The modulation period increases with the harmonic order because the pulse separation decreases.

To quantitatively compare the harmonic generation process in the laser field with time-dependent ellipticity with that in a linearly polarized laser field, the classical return times of electrons with different energy gains in the laser field with $E_x(t)$ in Eq. (1) were calculated [$E_y(t)=0$ was assumed, i.e., a linearly polarized field]. The energy gains correspond to the generation of harmonics with the same center frequencies as in Fig. 2(b). The results are shown in Fig. 2(c). In the same figure, the quantum return times that do take into account the effects of $E_y(t)$ are also shown. The quantum return times are the times of harmonic emission shown in Fig. 2(b). The good agreement between the classical and the quantum results indicates that harmonic generation process in the laser cycle around $t=0$ is very similar to that in a linearly polarized field. Since this emission time is different for harmonic pulses with different center frequencies, the harmonic pulses are chirped. The pulses corresponding to short trajectories are positively chirped, since the emission time increases with the central frequency. Alterna-

tively, the pulses corresponding to the long trajectories are negatively chirped because the emission time decreases with the central frequency. Both the positive and negative chirps are close to linear. Such chirp behavior is indeed similar to the chirp of the harmonic pulses generated in a linear field [22]. There is a one-quarter laser-cycle shift between the results in Fig. 2(c) as compared to those in [22], due to the carrier-envelope phase being $\pi/4$ for generating the spectra in Fig. 2(a). In [22], the phase is zero, as in the experiments with 5-fs linearly polarized laser pulses [7].

When the whole plateau and cutoff spectra are used to generate attosecond pulses, their durations are limited by the chirp. It is very difficult to compensate for the positive and negative chirp simultaneously. Luckily, harmonic emission from the long trajectory can be suppressed by phase matching during the propagation. The harmonic pulses obtained including the effects of propagation are shown in Fig. 2(d). It is clear that only the emissions from the short trajectories survived. The modulation depth of the 3D spectrum in Fig. 2(a) is much smaller than in the single-atom case because the interference does not occur with just one pulse. The remaining pulses are positively chirped. The chirp is close to linear because the emission time follows a straight line. Thus, it is anticipated that the chirp can be compensated by an optical device that introduces a negative chirp, in order to generate transform-limited attosecond pulses. This method has been proposed to compensate the chirp of attosecond pulses generated with linearly polarized laser fields [23].

As have been pointed out by Kim *et al.*, some filters exhibit negative dispersion in the xuv region [23]. Ideally, the second- and higher-order phases of the filter should be the opposite of the harmonic spectral phase. The harmonic spectral phase varies with the radial position at the exit of the target, as shown in Fig. 3(a). The linear phases are not included in the figure because they do not affect the pulse duration. The phases are dominated by the second-order terms, indicated by the quasiparabolic shapes. This is consistent with the quasilinear chirp in Fig. 2(d). It is interesting that for plateau harmonics, the differences between phases for different axial points are small. Thus it is possible to compensate the chirp for these points using only one filter. The harmonic intensities also vary along the radial direction, as shown in Fig. 3(b). It is clear that the major contribution comes from the region near the z axis. In Fig. 4(a), the on-axis harmonic spectral phase is compared with the phase of a Sn filter with 1 μm thickness. For clarity, the sign of the Sn phase is reversed. In the region between the 90th and 130th harmonic orders, the two phases are very close. On the lower-frequency side (harmonic orders less than the 90th), the mismatch between the two phases is not a problem since the intensity there is suppressed by the filter absorption, as indicated by the filter transmission curve. The effects of mismatch on the higher-frequency side (harmonic order larger than the 140th) can be reduced by setting the cutoff frequency at the desired value. This is how the laser intensity 1.4×10^{15} W/cm^2 is chosen. The harmonic spectrum after the Sn filter is shown in Fig. 4(b). It covers the region where the chirp of the harmonics can be relatively well compensated by the filter. The harmonic pulse after the filter is shown in Fig. 4(c), which is 58 as. The pulse has wings at the trailing edge, which is caused by phase variation for harmonic orders higher than the 140th. Increasing the laser intensity and filter thickness produces even shorter pulses, but the contrast between the peak intensity and the wing is reduced. It is worth pointing out that both the on- and the off-axis regions of the target are included in the simulation. As a comparison the results in [23] were obtained with one-dimensional propagation.

In conclusion, the chirp of the supercontinuum is almost the same as that of the harmonics generated by a linearly polarized field. The chirp is positive and close to linear. In a restricted spectral region, the chirp can be compensated by the material dispersion to yield single pulses as short as 58 as. The shortest pulse achievable is limited by mismatch of the phases between the high harmonics and filters. The generation of even shorter pulses calls for techniques that can introduce negative chirp over an even wider spectral region.

This work is supported by the Division of Chemical Sciences, Office of Basic Energy Sciences, U.S. Department of Energy.

[1] R. Kienberger, E. Goulielmakis, M. Uiberacker, A. Baltuska, V. Yakovlev, F. Bammer, A. Scrinzi, T. Westerwalbesloh, U. Kleineberg, U. Heinzmann, M. Drescher, and F. Krausz, Nature (London) **427**, 817 (2004).

[2] T. Brabec and F. Krausz, Rev. Mod. Phys. **72**, 545 (2000).

[3] P. Salieres, A. L'Huillier, Ph. Antoine, and M. Lewenstein, Adv. At., Mol., Opt. Phys. **41**, 83 (1999).

[4] M. Hentschel, R. Kienberger, Ch. Spielmann, G. A. Reider, N. Milosevic, T. Brabec, P. Corkum, U. Heinzmann, M. Drescher, and F. Krausz, Nature (London) **414**, 509 (2001).

[5] M. Drescher, M. Hentschel, R. Kienberger, G. Tempea, C. Spielmann, G. A. Reider, P. B. Corkum, and F. Krausz, Science **291**, 1923 (2001).

[6] M. Drescher, M. Hentschel, R. Kienberger, M. Uiberacker, V. Yakovlev, A. Scrinzi, Th. Westerwalbesloh, U. Kleineberg, U. Heinzmann, and F. Krausz, Nature (London) **419**, 803 (2002).

[7] A. Baltuska, Th. Udem, M. Uiberacker, M. Hentschel, E. Goulielmakis, Ch. Gohle, R. Holzwarth, V. S. Yakovlev, A. Scrinzi, T. W. Hansch, and F. Krausz, Nature (London) **421**, 611 (2003).

[8] P. Agostini and L. F. DiMauro, Rep. Prog. Phys. **67**, 813 (2004).

[9] Bing Shan, Shambhu Ghimire, and Zenghu Chang, J. Mod. Opt. **52**, 277 (2005).

[10] Zenghu Chang, Phys. Rev. A **70**, 043802 (2004).

[11] P. B. Corkum, N. H. Burnett, and M. Y. Ivanov, Opt. Lett. **19**, 1870 (1994).

[12] M. Ivanov, P. B. Corkum, T. Zuo, and A. Bandrauk, Phys. Rev.

Lett. **74**, 2933 (1995).
[13] P. Antoine, B. Piraux, D. B. Milosevic, and M. Gajda, Phys. Rev. A **54**, R1761 (1996).
[14] V. T. Platonenko and V. V. Strelkov, J. Opt. Soc. Am. B **16**, 435 (1999).
[15] V. Strelkov, A. Zair, O. Tcherbakoff, R. López-Martens, E. Cormier, E. Mével, and E. Constant, Appl. Phys. B: Lasers Opt. **78**, 879 (2004).
[16] E. Priori, G. Cerullo, M. Nisoli, S. Stagira, S. De Silvestri, P. Villoresi, L. Poletto, P. Ceccherini, C. Altucci, R. Bruzzese, and C. de Lisio, Phys. Rev. A **61**, 063801 (2000).
[17] M. Lewenstein, P. Balcou, M. Y. Ivanov, A. L'Huillier, and P. B. Corkum, Phys. Rev. A **49**, 2117 (1994).
[18] M. V. Ammosov, N. B. Delone, and V. Krainov, Zh. Eksp. Teor. Fiz. **91**, 2008 (1986) [Sov. Phys. JETP **64**, 1191 (1986)].
[19] F. A. Ilkov *et al.*, J. Phys. B **25**, 4005 (1992).
[20] A. de Bohan, P. Antoine, D. B. Milosevic, and B. Piraux, Phys. Rev. Lett. **81**, 1837 (1998).
[21] P. Antoine, A. L'Huillier, and M. Lewenstein, Phys. Rev. Lett. **77**, 1234 (1996).
[22] S. Kazamias and Ph. Balcou, Phys. Rev. A **69**, 063416 (2004).
[23] K. T. Kim, C. M. Kim, M.-G. Baik, G. Umesh, and C. H. Nam, Phys. Rev. A **69**, 051805(R) (2004).